PHYSICAL INSIGHT INTO THE UNSTEADY SHOCK-WAVE TURBULENT BOUNDARY LAYER INTERACTION USING LARGE EDDY SIMULATION

G. Aubard, J. C. Robinet, and X. Gloerfelt
DynFluid Laboratory
Arts et Métiers ParisTech
151, boulevard de l'Hôpital,
75013 Paris, France
guillaume.aubard@ensam.eu

ABSTRACT

Separated flows, characterized by the presence of a recirculation bubble and a shear-layer developping along the bubble, are often the seat of self-sustained low-frequency (LF) dynamics. The case of the shock-wave turbulent boundary layer interaction (SWTBLI) on a flat plate is analysed by means of LES simulations. A recent non-linear modal analysis, based on the 'dynamic mode decomposition' (DMD) is applied to an LES database. The typical LF modes are associated with a cyclic contraction and expansion of the recirculation bubble, taking the form of filling and emptying very close to the description of the mass-budget-based model proposed by Piponniau *et al.* (2009). The bubble is found to be divided into two zones, an upstream one associated with LF dynamics, and a downstream one associated with high-frequency 'Kelvin-Helmholtz-type' ('KH-type') vortices. When increasing the Strouhal number, the spatial support of the DMD modes moves continuously from the first part of the bubble to the entire bubble and the downstream flow.

INTRODUCTION

Separated flows appear in many configurations of technological interest, both in the incompressible and supersonic regimes. In both regimes, the separated zone is characterized by the presence of a recirculation bubble and a shear-layer developping along the bubble. These configurations are often the seat of self-sustained low-frequency (LF) dynamics. The origin of this LF activity is not fully understood, but many studies suggest that it is linked to the dynamics of the separated boundary-layer (Robinet (2007)).

Recent studies, in the incompressible regime, have shown that a boundary layer could generate a LF dynamics resulting from the interaction of the instability waves developing in the shear-layer (Cherubini *et al.* (2010)). Indeed, global instability analyses have shown that beyond some threshold in physical characteristics of the separated zone (bubble aspect ratio, backflow intensity) the flow becomes unstable. When more than two shear-layer modes are unstable, LF vortex-shedding appears. The LF activity is mainly localized in the downstream part of the bubble.

In the supersonic regime, the separation zone can be generated by the impact of a shock-wave on a developping boundary layer. If the pressure jump across the incident shock is sufficiently large, the associated adverse pressure gradient leads to the separation of the incoming boundary layer which forms a separation bubble. The deflection of the flow away from the wall generates compression waves which form the reflected shock. At the top of the bubble, an expansion fan is produced, followed by weak compression waves near reattachment. Finally, downstream of the interaction, the boundary layer is subject to a relaxation zone. Beyond some threshold, notably in the angle of impact of the incoming shock, this 'reflected shock / separation bubble' configuration is often the seat of LF motions (Dolling (2001)).

The LF activity, often identified by the fore-and-aft motion of the reflected shock, but also associated with a "breathing" motion of the separation bubble, shows similarities with the incompressible regime. It seems therefore legitimate to search if a similar mechanism could govern the LF dynamics for both regimes. In the compressible turbulent regime, two scenarios have been recently proposed. The first one, proposed by Piponniau *et al.* (2009), links the LF activity to the shear-layer developping along the separation line. A simple model, based on a mass-budget of the separated region, has been developed. The vortices shed in the shear-layer fill the bubble until a critical mass is reached. The mass-flow inside the bubble is then ejected into the downstream flow. These successive gain and loss of mass create a low-frequency cyclic contraction and expansion of the bubble, which timescale is estimated to be close to the LF motion of interest. The second scenario, proposed by Touber & Sandham (2011), suggests that the LF motion comes from a selective response of the reflected shock foot to a random forcing. Following the idea of Plotkin (1975), they argue that the shock displacement is obeing a first order stochastic Ordinary Differential Equation with an associated timescale. The shock then simply amplifies low-frequencies already present in the incoming flow and is responsible alone for the LF activity in the separation region.

A recent non-linear modal analysis has been proposed by Schmid (2010) and Rowley *et al.* (2010). This method, based on the 'dynamic mode decomposition' (DMD), allows the extraction of dynamically relevant flow features using only time-resolved numerical data. We propose in this paper to apply this algorithm on an LES database of a shock-wave turbulent boundary layer interaction (SWTBLI) on a flat plate. The idea is to visualize the spatial structure associated with the LF modes and to relate it with current knowledge on the issue of flow unsteadiness. The numerical strategy adapted to compressible flows is described and validated in the first section. Then the LES database with the flow conditions is presented. The non-linear spectral analysis is then detailed and discussed. The main conclusions are given in the last section.

NUMERICAL METHODS AND FLOW PARAMETERS

Numerical discretization

The need to resolve the fine turbulent scales and to capture several periods of the low-frequency oscillation of the reflected shock implies the use of low cost numerical algorithms. The LES strategy used in this study combines a finite-difference scheme with good spectral properties with the use of a selective filtering without an additional eddy-viscosity model. The high-order explicit filtering provides a smooth defiltering by removing the fluctuations at wavenumbers greater than the finite-difference scheme resolvability, and provides the necessary regularization at small scales. An important advantage of the LES strategy is that no additional effort is required, whereas more elaborate models can induce 20% to one order of additional cost. The time integration is done using an explicit low-storage optimized six-step Runge-Kutta scheme.

Nonreflecting characteristic boundary conditions are used at the outflow and at the top boundary. The shock is introduced at the inflow boundary using the inviscid Rankine-Hugoniot jump conditions. The wall temperature is calculated with the adiabatic condition. Periodicity is assumed in the spanwise direction.

The Synthetic Eddy Method (SEM) in the form proposed by Pamies *et al.* (2009) is used to generate realistic time dependent inflow conditions for the LES simulations. The adaptation distance needed to recover a realistic wall turbulence, estimated using notably the longitudinal evolution of the *rms* velocities is found to be smaller than $10\delta_0$ (where δ_0 is the inflow boundary layer thickness based on 99% of the external velocity). Moreover, this methodology does not introduce any periodicity in the flow, which is particularly important in this study.

The centered finite-difference schemes used in this study have no shock-capturing features, so that when encountering flow with discontinuities, they may fail to describe the solution because of their inability to deal with the spurious oscillations generated by the Gibbs phenomenon. This issue is circumvented here by employing the Adaptative Nonlinear Selective Filtering (ANSF) where a signal processing operation is applied after each time step in order to adjust the solution near discontinuities. The amplitude of the filtering is adjusted dynamically using the fluctuations of dilatation, and the original method is coupled to a Ducros sensor to improve the selectivity of the shock-capturing device.

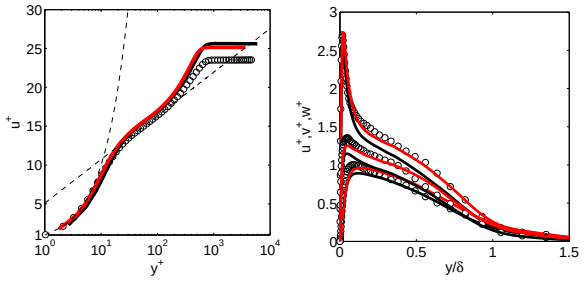

Figure 1. Van Driest transformed mean velocity profiles (left), and *rms* profiles normalized by the friction velocity (right) : (———), "coarse" LES; (———), "fine" LES; (○), DNS of Pirozzoli *et al.* (2004).

Validation of the numerical strategy

Undisturbed turbulent boundary layer The Direct Numerical Simulation (DNS) of a turbulent boundary layer of Pirozzoli *et al.* (2004) at free-stream Mach number $M_\infty = 2.25$ and Reynolds number $Re_\theta = 4260$ is reproduced in order to validate the turbulent inflow boundary condition. Two grids are tested : a "coarse" one ($\Delta_x^+ = 39$, $\Delta_{y_{min}}^+ = 2.9$, $\Delta_z^+ = 18$), and a "fine" one ($\Delta_x^+ = 33$, $\Delta_{y_{min}}^+ = 1.7$, $\Delta_z^+ = 13$).

Figure 1 shows van Driest transformed mean velocity profiles in good agreement with the DNS, despite an underestimation of the friction velocity less than 10%, which is customary using LES resolutions. The *rms* profiles are slighty underestimated by the "coarse" grid (in black) but are in very good agreement with the DNS for the "fine" grid (in red).

Shock interaction The SWTBLI case of Pirozzoli & Grasso (2006) at free-stream Mach number $M_\infty = 2.25$ and Reynolds number $Re_\theta = 3725$ is reproduced in order to validate the numerical strategy. The incidence angle of the shock generator is 8°.

The computational domain has a size of $Lx \times Ly \times Lz = 20\delta_0 \times 11\delta_0 \times 3\delta_0$. It is discretized with a grid consisting of $400 \times 200 \times 154$ points. The grid points are uniformly spaced in the streamwise and spanwise direction, and are clustered in the wall-normal direction according to a geometric progression of 2%. Evaluated upstream of the interaction, the resolution in term of wall units is $\Delta_x^+ = 35$, $\Delta_y^+ = 1.7$, $\Delta_z^+ = 14$. The time step is $0.0023\delta_0/U_\infty$. After an initial transient of $1200\delta_0/U_\infty$, the time span of the computation is $800\delta_0/U_\infty$.

Figure 2 shows the longitudinal evolution of the friction coefficient (left) and the wall-pressure (right) in a coordinate system centered on the reattachment point x_{reat} and normalized by the separation length L_{sep} (defined as the distance between the mean separation point and the mean reattachment point). The friction coefficient is in very good agreement with the DNS. The wall-pressure jump is surprisingly sharper in the LES simulation even the downstream flow conditions are well recovered. It is worth noticing that an other LES has been performed recently on the same configuration, and similar discrepansies with the DNS of Pirozzoli & Grasso (2006) have been observed (Petrache *et al.* (2010)).

Figure 3 shows mean velocity profiles at various streamwise stations. The profiles reasonably match the DNS except in the upstream part of the boundary layer just after the recir-

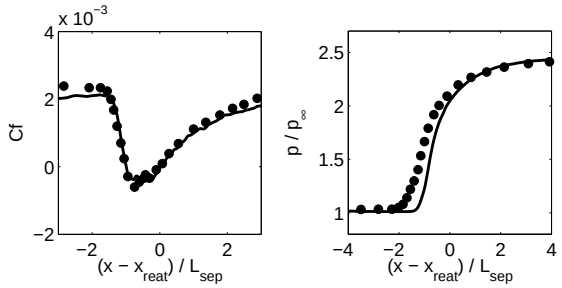

Figure 2. Longitudinal evolution of the friction coefficient (left) and of the wall-pressure jump (right) : (———), LES; (○), DNS of Pirozzoli & Grasso (2006).

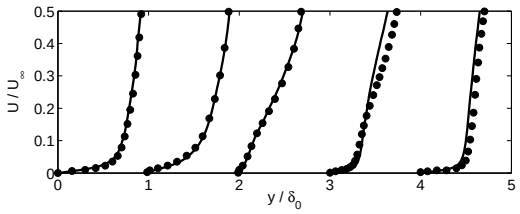

Figure 3. Mean velocity profiles at streamwise stations $(x - x_{reat})/L_{sep} = -2, -1, -0.5, 1.5, 6.$: (———), LES; (○), DNS of Pirozzoli & Grasso (2006).

culation bubble.

FLOW ANALYSIS

Linear spectral analysis

The shock angle chosen in the previous section leads to a weakly separated boundary layer. Therefore, an other LES simulation of SWTBLI has been performed with the same flow conditions and numerical discretization but with an incidence angle of the shock generator of 9°. This generates a stronger interaction and therefore a larger separation bubble.

The calculation has been advanced in time until statistical steadiness is achieved. Then, samples of wall-pressure field have been collected at time intervals of $0.121\delta_0/U_\infty$. The time span of the simulation guaranties a frequency resolution of the order of $0.000275U_\infty/\delta_0$ which corresponds to a Strouhal number based on L_{sep} of 0.0009 ($St = fL_{sep}/U_\infty$).

At this point, we introduce the following nondimensional coordinate system, centered on the separation point and normralized by L_{sep} : $x = (x - X_{sep})/L_{sep}$, and $y = y/L_{sep}$.

Figure 4 shows the longitudinal evolution of the pre-multiplied wall-pressure spectra as a function of the Strouhal number. Most of the low-frequency energy content is localized near the separation point (black dashed line). This behaviour is different from incompressible results, where the LF activity is concentrated near the reattachment point (associated with LF vortex-shedding). The shift observed downstream of the reflected shock foot is associated with the thickening of the boundary layer and the generation of 'KH-type' structures by the shear-layer.

Figure 5 shows the pre-multiplied wall-pressure spectra as a function of the Strouhal number at a position located near

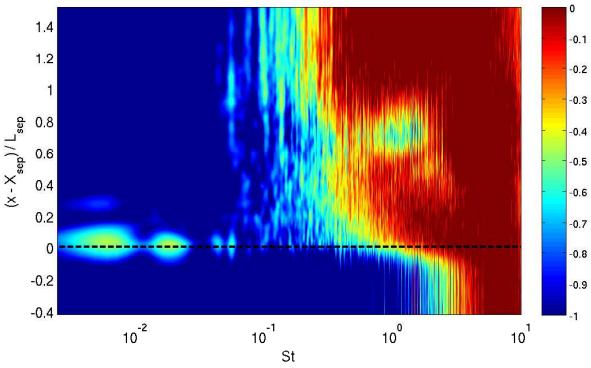

Figure 4. Longitudinal evolution of the logarithm of the pre-multiplied wall-pressure spectra as a function of the Strouhal number. The spectra are normalized so that their integral over frequency is unity for each station.

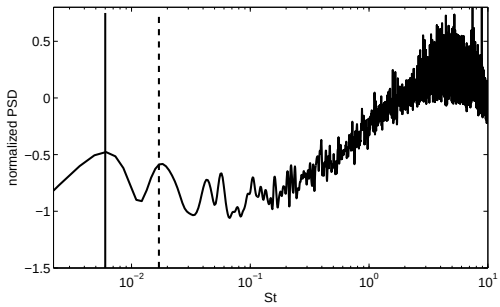

Figure 5. Pre-multiplied pressure wall-spectra as a function of the Strouhal number at a position near the separation point.

the separation point. The LF activity is associated with a bump in terms of Strouhal numbers instead of a single peak. This bump is centered near $St = 0.006$ (black straight line). A secondary LF peak is also visible around $St = 0.02$ (black dashed line). A ratio L_{sep}/δ_0 of 4.05 is obtained in this simulation. This result is very close to the experimental value of 4.2 obtained by Piponniau *et al.* (2009). However δ_0 is six times smaller in our simulation. That explains why the Strouhal number $St = fL_{sep}/U_\infty$ associated with the LF bump is almost six times smaller than the value of 0.03 obtained by Piponniau *et al.* (2009) for the same incident shock angle.

Low-pass filtering is applied to the pressure fluctuations field with a cutoff Strouhal number of 0.02. The corresponding filtered field is shown on Fig.6. The incident and reflected shock are indicated by the black dashed lines, and the sonic line by the pink dashed line. The figure suggests that above the sonic line, the LF activity is concentrated on two distinct zones : the reflected shock and the expansion fan.

Non-linear spectral analysis

To analyze the nonlinear dynamics, a new method is used based on spectral analysis of the Koopman operator. The Koopman operator is a linear operator defined for any nonlinear system, but it is not based on linearization: indeed, it captures all of the dynamics of the full nonlinear system. The

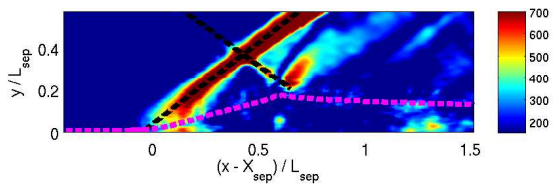

Figure 6. Low-pass filtered pressure fluctuations field with cutoff Strouhal number 0.02.

Koopman operator describes the evolution of observables on the phase space. The governing equations are regarded as the dynamical system as follows:

$$\mathbf{u}_{k+1} = \mathbf{F}(\mathbf{u}_k)$$

where $\mathbf{u}$ is state vector, k is the time increment and $\mathbf{F}$ is the Navier-Stokes operator. To analyse the flow dynamics only from time-resolved snapshots amounts to computing the following eigenproblem $\mathscr{K}\phi_j(\mathbf{u}) = \lambda_j\phi_j(\mathbf{u})$ where ϕ_j and λ_j are the eigenfunctions and eigenvalues of the Koopman operator $\mathscr{K}$ respectively. This operator has the following properties: For all observable physical quantities $\mathbf{q}$, the Koopman operator acting on $\mathbf{q}(\mathbf{u}_k)$ as $\mathscr{K}\mathbf{q}(\mathbf{u}_k) = \mathbf{q}(\mathbf{F}(\mathbf{u}_k)) = \mathbf{q}(\mathbf{u}_{k+1})$ or $\mathscr{K}^k\mathbf{q}(\mathbf{u}_0) = \mathbf{q}(\mathbf{u}_k)$. $\mathbf{q}(\mathbf{u}_k)$ may be expanded in terms of these eigenfunctions, as

$$\mathbf{q}(\mathbf{u}_k) = \sum_{j=1}^{\infty}\phi_j(\mathbf{u}_k)\mathbf{v_j} = \sum_{j=1}^{\infty}\mathscr{K}^k\phi_j(\mathbf{u}_0)\mathbf{v_j} = \sum_{j=1}^{\infty}\lambda_j^k\phi_j(\mathbf{u}_0)\mathbf{v_j}$$

where the eigenfunctions ϕ_j and the corresponding vectors $\mathbf{v_j}$ as the Koopman eigenfunctions and Koopman modes of the map $\mathbf{F}$, corresponding to the observable $\mathbf{q}$. Approximate Koopman eigenvalues λ_j and eigenvectors $\mathbf{v_j}$ are computed from a sequence of flow-fields $\{\mathbf{u}_0, \mathbf{u}_1, ..., \mathbf{u}_{m-1}\}$ with a given number of snapshots m and time interval Δt. The corresponding frequencies are given by $\omega_j = \Im\left[log(\lambda_j)\right]/\Delta t$. The following scalar product is used to project the dynamics on a lower-dimensional space :

$$\iint\left[\frac{\rho u_i'^2}{2} + \frac{p'^2}{2\gamma\overline{P}} + \frac{(\gamma-1)\overline{P}s'^2}{\gamma r^2}\right]dxdy$$

where s is the thermodynamic entropy, and $r = c_p - c_v$ is the gas constant. The computation of Koopman modes from snapshots is realized by the DMD algorithm which is precisely described by Schmid (2010). Due to memory limitations, the DMD method is applied only to two-dimensional snapshots of the fluctuations flow variables in a first time. The snapshots are taken in the sub-domain $x \in [-0.4, 1.5]$, $y \in [0., 0.6]$ in the nondimensional coordinate system defined in the previous section. The domain is large enough to include the incoming boundary layer, the recirculation bubble, and the dowstream flow. 3850 snapshots spaced at intervals of $\Delta t U_\infty / L_{sep} = 0.0949$ are collected, for a maximum resolvable Strouhal number of 10.5 and a minimum resolvable Strouhal number of 0.0027.

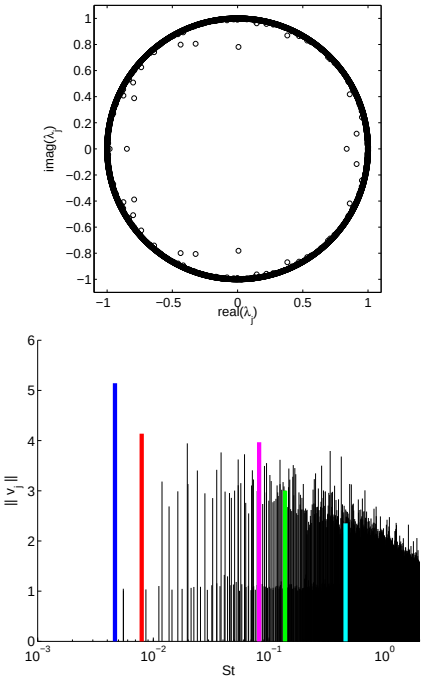

Figure 7. Top : Spectrum of the approximate Koopman eigenvalues λ_j. Bottom : Magnitude of the Koopman modes as a function of the Strouhal number.

Figure 7 (top) shows the spectrum of the approximate Koopman eigenvalues λ_j. Almost all eigenvalues lie on the unit circle, indicating that the dynamics is statistically stationary.

The magnitude of the Koopman modes, defined by the global energy norm $\|\mathbf{v_j}\|$, are shown on Fig.7 (bottom) as a function of the Strouhal number (in a logarithmic scale). The turbulent nature of the flow generates a continuous field of peaks ranging from high to low frequencies. The modes associated with the LF dynamics are however clearly visible. The modes associated with the colored peaks are considered in this section.

The shape of a LF mode (blue peak on Fig.7 (bottom), $St = 0.006$) is shown on Fig.8 for equally spaced phase intervals of a quarter of period. The mean field is also added. The sonic line is indicated by a black dashed line.

The LF mode clearly exhibits a global breathing motion of the recirculation bubble. More precisely, the mass of fluid amount in the bubble starts to increase in the upstream part of the interaction zone (from the separation point to the incident shock impact on the boundary layer), probably entrained by the mixing layer. The mass amount is then shedded into the downstream flow, decreasing the size of the bubble. Then, the bubble size starts to increase again from the shear-layer. This behaviour is obtained by a modal decomposition, and therefore cannot be associated directly to a physical structure present in the flow. However, this cyclic contraction and expansion of the bubble corresponds to a physical dynamics that is observed in experiments and numerical simulations.

The shape of a typical high-frequency mode (cyan peak on Fig.7 (bottom), $St = 0.45$) is shown on Fig.9. Most of the high-frequency activity is localized along the sonic line and

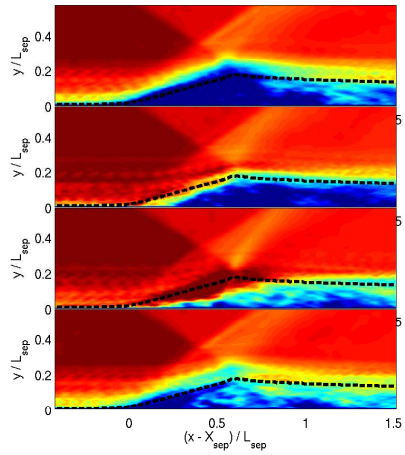

Figure 8. Contours of u' for a LF mode close to $St = 0.006$; (blue peak on Fig.7 (bottom)).

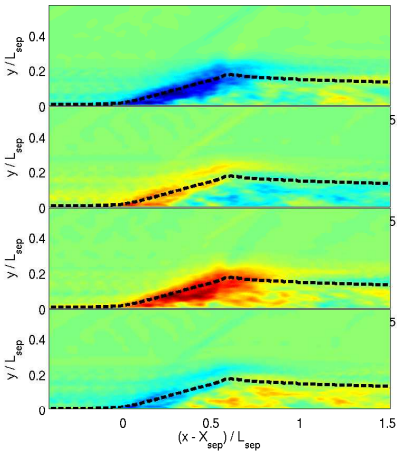

Figure 10. Contours of u' for a mode close to $St = 0.006$; (blue peak on Fig.7 (bottom)).

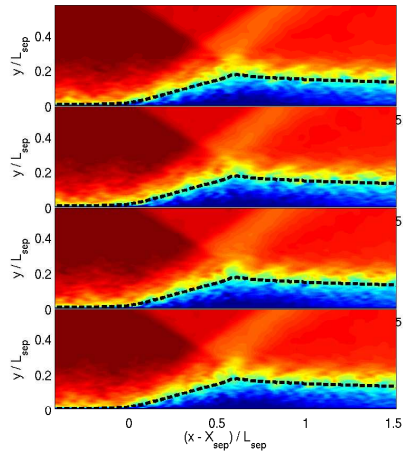

Figure 9. Contours of u' for a high-frequency mode close to $St = 0.45$; (cyan peak on Fig.7 (bottom)).

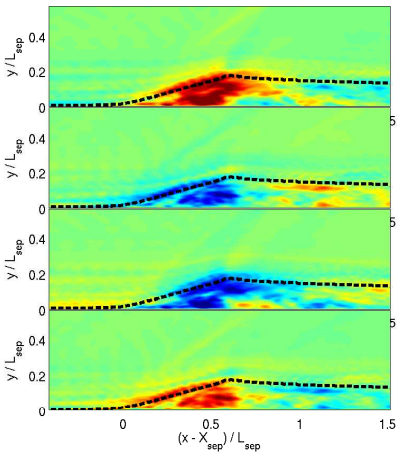

Figure 11. Contours of u' for a mode close to $St = 0.0075$; (red peak on Fig.7 (bottom)).

does not affect the size of the recirculation bubble, suggesting that high and low frequency dynamics are decoupled.

Figure 10 to Figure 14 show the shape of DMD modes for increasing the Strouhal numbers $St = 0.006$, 0.0075, 0.02, 0.14, and 0.45. It appears clearly that the spatial support associated with a typical LF mode is concentrated in the upstream part of the recirculation bubble. When increasing the Strouhal number, the support progressively fills the rest of the bubble and the downstream flow. Moreover, it is rapidly located along the sonic line, turning continuously into 'KH-type' vortices of increasing frequencies (Fig.12 and Fig.13).

CONCLUSIONS

For one of the first time (Pirozzoli *et al.* (2010)), a recent 'non-standard' modal decomposition method based on the DMD algorithm has been applied to the unsteady SWT-BLI case. Three main observations can be made from this analysis :

1. The spatial support of a typical LF mode is concentrated in the first part of the recirculation bubble, mainly along the shear-layer. This observation is in good agreement with the scenario proposed by Touber & Sandham (2011) where the LF dynamics is localized near the reflected shock foot. It clearly shows that the bubble is divided into two zones, an upstream one associated with LF dynamics, and a downstream one associated with higher-frequency 'KH-type' vortex shedding.
2. The temporal reconstruction of the LF modes reveals a cyclic filling and emptying of the bubble that is very close to the mass-budget-based model proposed by Piponniau *et al.* (2009).
3. Finally, when increasing the Stouhal number, the spatial support of the DMD modes fills the rest of the bubble and the downstream flow. It's however interesting to note that this evolution is continuous and progressive.

A next step would be to apply the DMD on three-dimensional snapshots, because the separation zone, and the KH generated by the shear-layer, could be three-dimensional (Robinet (2007)).

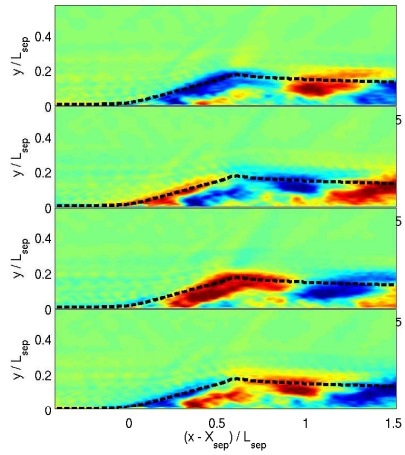

Figure 12. Contours of u' for a mode close to $St = 0.02$; (pink peak on Fig.7 (bottom)).

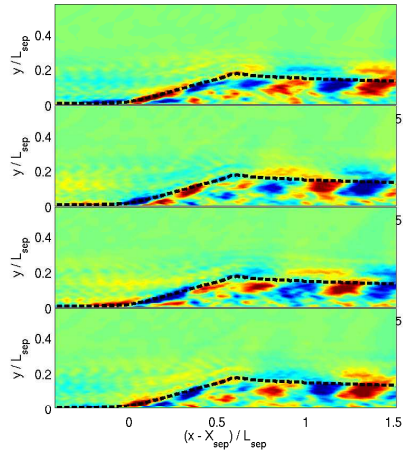

Figure 13. Contours of u' for a mode close to $St = 0.14$; (green peak on Fig.7 (bottom)).

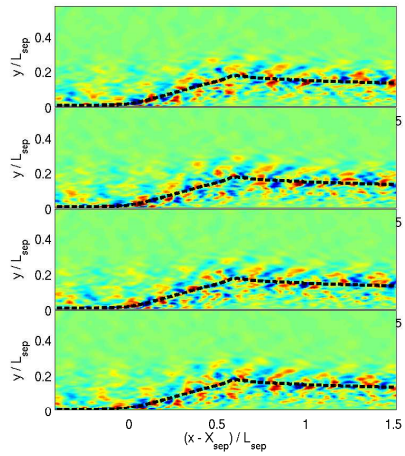

Figure 14. Contours of u' for a mode close to $St = 0.45$; (cyan peak on Fig.7 (bottom)).

This work was granted access to the HPC resources of IDRIS and CCRT under the allocation 2010-6125 made by GENCI (Grand Equipement National de Calcul Intensif). The authors gratefully acknowledge the support of the Agence Nationale de la Recherche under the project SPICEX (ANR-07CIS7-009).

REFERENCES

Cherubini, S., Robinet, J.-Ch. & De Palma, P. 2010 The effects of non-normality and non-linearity of the Navier-Stokes operator on the dynamics of a large laminar separation bubble. *Phys. Fluids* **22** (01), 014102.

Dolling, D. S. 2001 Fifty years of shock-wave/boundary-layer interaction research: What next? *AIAA Journal* **39** (8).

Pamies, M., Weiss, P.E., Garnier, E., Deck, S. & Sagaut, P. 2009 Generation of synthetic turbulent inflow data for large eddy simulation of spatially evolving wall-bounded flows. *Phys. Fluids* **21** (4), 045103–045118.

Petrache, O.C., Hickel, S. & Adams, N.A. 2010 Implicit LES of shock-turbulent boundary layer interaction. In *8th Euromech Fluid Mechanics Conference (EFMC8)*. Bad Reichenhall, Germany.

Piponniau, S., Dussauge, J.P., Debieve, J.F. & Dupont, P. 2009 A simple model for low-frequency unsteadiness in shock-induced separation. *J. Fluid Mech.* **629**, 87–108.

Pirozzoli, S. & Grasso, F. 2006 Direct numerical simulation of impinging shock wave/turbulent boundary layer interaction at $M = 2.25$. *Phys. Fluids* **18** (6), 065113–065130.

Pirozzoli, S., Grasso, F. & Gatski, T.B. 2004 Direct numerical simulation and analysis of a spatially evolving supersonic turbulent boundary layer at $M = 2.25$. *Phys. Fluids* **16** (3), 530–545.

Pirozzoli, S., Larsson, J., Nichols, J. W., Bernardini, M., Morgan, B. E. & Lele, S. K. 2010 Analysis of unsteady effects in shock/boundary layer interactions. *Proceedings of the Summer Program, Center for Turbulence Research* .

Plotkin, K. J. 1975 Shock wave oscillation driven by turbulent boundary-layer fluctuations. *AIAA Journal* **13** (8).

Robinet, J.-Ch. 2007 Bifurcations in shock wave / laminar boundary layer interaction: Global instability approach. *J. Fluid Mech.* **578**, 67–94.

Rowley, C.W., Mezic, I., Bagheri, S., Schlatter, P. & Henningson, D.S. 2010 Spectral analysis of nonlinear flows. *J. Fluid Mech.* **641**, 115–127.

Schmid, P.J. 2010 Dynamic mode decomposition of numerical and experimental data. *J. Fluid Mech.* **656**, 5–28.

Touber, E. & Sandham, N.D. 2011 Low-order stochastic modelling of low-frequency motions in reflected shock-wave/boundary-layer interactions. *J. Fluid Mech.* **417** (465).